Materials Advances

ROYAL SOCIETY OF CHEMISTRY

PAPER

View Article Online
View Journal | View Issue

Cite this: *Mater. Adv.*, 2026, 7, 3875

Tailoring lithium dicyanoimidazolide: structure–property relationships

Daniel Pokorný,[a] Tomáš Syrový,[b] Milan Klikar,[a] Patrik Pařík,[a] Zuzana Burešová,[a] Lenka Řeháčková[c] and Filip Bureš *[a]

Taking lithium 2-trifluoromethyl-4,5-dicyanoimidazol-1-ide as a parent lithium salt for Li-ion batteries, systematic property tuning in two series based on variously 2- and 4-substituted 4,5-dicyanoimidazolide and 2-phenyl-4,5-dicyanoimidazolide scaffolds is demonstrated. A straightforward synthetic approach afforded fourteen desired derivatives with a systematically evaluated structure, whose properties were further investigated from various perspectives. The stabilization of the imidazolide anions *via* the substituent effects was examined using dissociation constants, the Hammett equation, ^{13}C NMR shifts and electronic absorption spectra. Solubility in dimethyl carbonate and 1,2-dimethoxyethane further identified lithium salts with a potential for a practical application, and their solutions were further investigated for aggregation phenomena. Using absorption spectroscopy, a significantly more sensitive and straightforward methodology is presented, which allows the identification of perspective substituents hindering aggregation. The viscosity and density measurements further confirmed the significant property tuning of electrolytes upon changing the structure of lithium dicyanoimidazolide, which is in line with the subsequent electrochemical measurements. Based on the complete gathered data, extension *via* the 1,4-phenylene moiety along with peripheral (O)CF_3-substitution proved to be a useful strategy towards stabilized anions with a promising application in lithium-ion batteries.

Received 9th February 2026,
Accepted 3rd March 2026

DOI: 10.1039/d6ma00187d

rsc.li/materials-advances

Introduction

The growing demand for portable power sources has made lithium-ion batteries (LIBs) a cornerstone of modern technology, especially in consumer electronics. Nowadays, these batteries power everything from smartphones and laptops to electric vehicles, providing a lightweight and efficient energy solution.[1–3] Despite the evolution in time and the recent advancements, the core technology remains unaltered, in which the lithium cation (Li^+) is used as a primary charge carrier, benefiting from its reversible redox process occurring at the most negative potential (−3.04 V *vs.* SHE). Inorganic lithium salts such as $LiPF_6$ and $LiBF_4$ are considered conventional electrolytes, nevertheless suffering from some stability and safety issues.[4–8] Considering the electrolyte a crucial part of batteries, these limitations drive the ongoing efforts to identify alternative salts. The vast majority of commercial LIBs utilize non-aqueous electrolytes; in particular dipolar aprotic solvents or ionic liquids are used. The counterion to Li^+ acts as a stabilizing agent, ensuring its dissociation, while being chemically inert and resistant to the (electro)chemical environment of batteries. Overall, an idealized electrolyte of LIBs combined with an organic solvent should (i) assure free movement of lithium (ions) between electrodes, (ii) exhibit high ionic conductivity and minimal internal resistance, (iii) possess electrochemical and (iv) thermal stability (avoiding degradation across the operating voltage/temperature window) and (v) allow the efficient formation of a solid–electrolyte interface (SEI) to ensure stable and efficient interaction between the electrolyte and the electrodes.[9–11] Besides these fundamental criteria, the electrolyte should be collector-friendly (non-corrosive), low in viscosity (within the operating temperature range), safe, environmentally friendly and cost-effective. Hence, various anions with the negative charge distributed over the boron and nitrogen atoms, exhibiting improved electrochemical performance and thermal robustness, were developed. For instance, these include borates[12,13] and imides such as lithium bis(fluorosulfonyl)imide (LiFSI)[14] and bis(trifluoromethanesulfonyl)imide (LiTFSI).[15] More recently, the concept of stable Hückel anions benefiting from significant stabilization through covalently bonded electron-acceptor moieties has been extended towards nitrogen heterocycles.[16,17] Five-membered 1*H*-imidazole and 1*H*-triazole proved to be the leading structural motives in designing such anions, and lithium 2-trifluoromethyl-

[a] *Institute of Organic Chemistry and Technology, Faculty of Chemical Technology, University of Pardubice, Studentská 573, Pardubice 53210, Czechia. E-mail: filip.bures@upce.cz*
[b] *Department of Graphic Arts and Photophysics, Faculty of Chemical Technology, University of Pardubice, Doubravice 41, Pardubice 53353, Czechia*
[c] *Department of Chemistry and Physico-Chemical Processes, Faculty of Materials Science and Technology, VSB-Technical University of Ostrava, 17. listopadu 2172/15, Ostrava-Poruba 70800, Czechia*

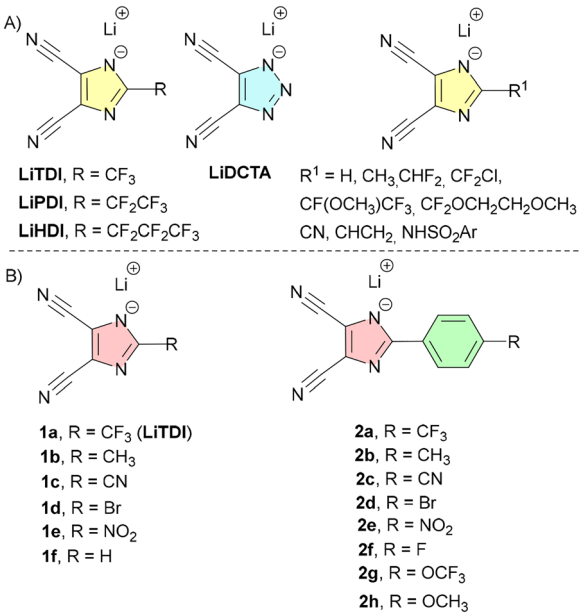

Fig. 1 Molecular structure of the known **LiTDI** (and its analogues **LiPDI** and **LiHDI**), **LiDCTA** and further C2-variations of imidazole-4,5-dicarbonitrile (A). Molecular structure of the investigated (2-phenyl)imidazole-4,5-dicarbonitrile derivatives **1** and **2** (B).

4,5-dicyanoimidazol-1-ide (**LiTDI**, Fig. 1A) and lithium 4,5-dicyanotriazol-1-ide (**LiDCTA**, Fig. 1A) represent the most typical examples. While **LiDCTA** was utilized in polymer electrolytes,[18–20] the synthesis of **LiTDI** was first reported by Bukowska *et al.*,[21] and its application in LIBs has further been extended by Niedzicki *et al.*[21–25] and Berhaut *et al.*[26,27] **LiTDI** has been reported to enable the formation of an efficient SEI,[28] while it may also be employed as a highly efficient additive to $LiPF_6$-based electrolytes by suppressing its hydrolysis.[29] Triple functionalization of the central imidazol-1-ide proved to be the key structural feature of **LiTDI**. While the two electron-withdrawing cyano groups at positions C4 and C5 improve the anion stability and weaken the Li^+ coordination, their linear arrangement allows maintaining a small molecular size with high solubility. The CF_3 group at position C2 enhances the intrinsic anion oxidation potential and lowers the HOMO energy, thus increases the HOMO–LUMO gap as compared to CH_3^- and H-substituted analogues.[30] Its electron-withdrawing property along with the bulky spatial arrangement, analogous to the isopropyl group, further extends the bond length between the ion pair, which reduces the ion pair dissociation energy and results in higher ionic conductivity. The quantum-chemical computational studies showed that replacement of the CF_3 group by longer perfluorinated chains (*e.g.* C_2F_5, C_3F_7) has only minimal impacts.[31,32]

Compared to a practically unfeasible structural variation of **LiDCTA**, further modification of **LiTDI** was carried out exclusively *via* an extension of the C2-appended trifluoromethyl group to perfluoroethyl (**LiPDI**) and perfluoropropyl ones (**LiHDI**), see Fig. 1A.[22–24,33] However, their practical application is constrained by the increased cost and availability of perfluorinated starting materials. When going from **LiTDI** to **LiHDI**, the elongated perfluoroalkyl chains bring an increase in viscosity due to the formation of stronger ion pairs and larger aggregation. However, the conductivity and ionicity of **LiHDI** and **LiPDI** in carbonates significantly exceed those of **LiTDI**. The structure of parent **LiTDI** was further explored less extensively, especially by utilizing commercially available derivatives such as (2-amino)imidazole-4,5-dicarbonitriles. Screening the portfolio of currently available patents reveals that the original CF_3 group of **LiTDI** can be replaced by hydrogen, methyl,[34] additional perfluoroalkyl(ether),[35] cyano,[36] and vinyl groups[37] as well as sulfonamides bearing various Ar pendants (Fig. 1A).[38] In addition, Rasmussen *et al.* reported tetracyanobiimidazole, however not intended for LIBs.[39]

The chemistry of imidazole-4,5-dicarbonitrile (dicyanoimidazole, DCI) was well explored by our group, as it has been introduced as a heterocyclic electron-withdrawing unit of various push–pull molecules with tunable optoelectronic properties and manifold applications.[40–44] Hence, we herewith demonstrate our systematic approach towards structural variation and property tuning of **LiTDI** by designing two series **1** and **2** (Fig. 1B), whereas the series **1a–f** consists of the imidazole-4,5-dicarbonitrile derivatives, the series **2a–h** is based on the parent 2-phenylimidazole-4,5-dicarbonitrile scaffold. An extension of the π-systems by the 1,4-phenylene moiety[45,46] is herewith proposed to stabilize the TDI^- anion. Further stabilization is accomplished by appending the substituent R featuring various inductive and/or mesomeric effects, including donors (CH_3, OCH_3, OCF_3, and Br) and acceptors (CF_3, CN, and NO_2). In series **2**, the substituents are appended in position 4 of the phenyl ring to utilize the whole conjugated pathway and maintain the molecular symmetry. 1,4-Phenylene moiety in **2a–h** also assures better distancing of the imidazolide anion and the R functional group and potentially reduces the crystal lattice energy of the lithium salt, especially when R contains electronegative fluorine.[10] Moreover, fluorine-containing groups generally improve solubility and stability in solutions.

Results and discussion

Synthesis

The lithium salts **1a–f** and **2a–h** were synthesized *via* a general two-step protocol, as outlined in Scheme 1 (see the SI for complete synthetic details). While the parent 1*H*-imidazoles **3f** and **3g** are commercially available, remaining 1*H*-imidazole-4,5-dicarbonitrile derivatives **3** and **4** were synthesized. The cyclocondensation of diaminomaleonitrile (DAMN, **5**) with trifluoroacetic anhydride (TFAA) or triethylorthoacetate afforded 1*H*-imidazoles **3a** and **3b**, while electrophilic bromination of **3f** or diazotization/Sandmeyer reactions with **3g** provided derivatives **3c**, **3d** and **3e**. DAMN can be also treated with substituted benzaldehydes **8a–h** towards imine intermediates **7a–h** that were cyclized under oxidative conditions to 1*H*-imidazoles **4a–h**. This way prepared NH-acids **3** and **4** were subsequently reacted with LiH to yield the desired lithium salts **1** and **2** (Scheme 1B). The lithiation and all further treatment of **1** and **2**

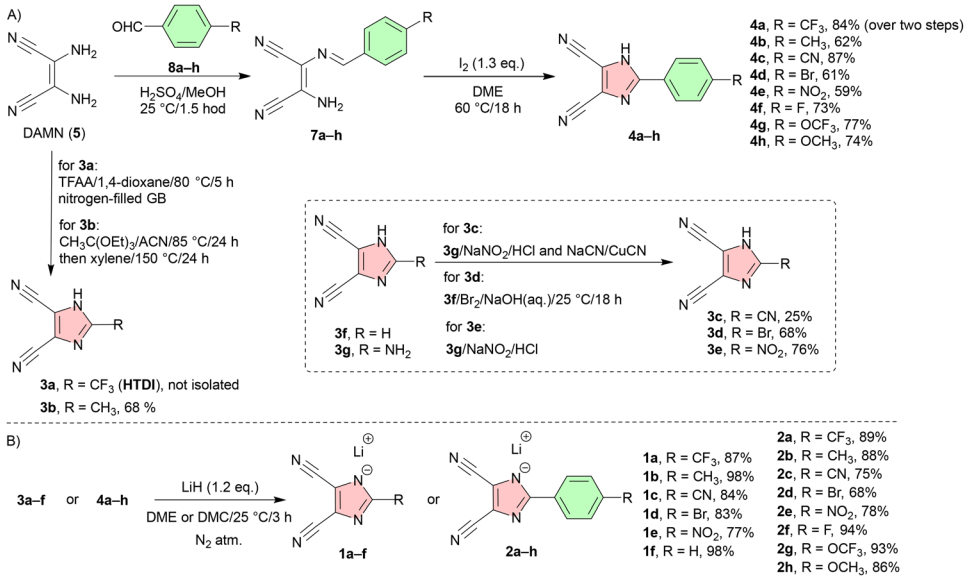

Scheme 1 Synthetic strategy of 1*H*-imidazoles (**3** and **4**) (A) and their neutralization to lithium salts (**1** and **2**) (B).

were carried out in a nitrogen-filled glovebox due to their high hygroscopicity.

Substituent effects

To quantify the varied substitution patterns in 1*H*-imidazoles **3** and **4** and the extent of the charge delocalization in the corresponding imidazolides **1** and **2**, dissociation constants (pK_a) were determined *via* potentiometric titration (Table 1).[47–49] Two solvents were used, protic methanol (MeOH) and aprotic acetonitrile (ACN). Having the same 1*H*-imidazole-4,5-dicarbonitrile moiety in all derivatives **3**, the variation in the acidity is ascribed to the electronic effects of the substituent appended at the position C2. When going from the parent **HTDI** (**3a**, pK_a = 3.71/10.96 in MeOH/ACN) to C2-unsubstituted (**3f**) and methyl-substituted (**3b**) derivatives, the acidity decreases by five/seven orders of magnitude as a result of removing the CF_3 inductive acceptor and attaching hydrogen or the CH_3 donor.

The highest acidity was measured for tricyanoimidazole **3c**, which reflects attachment of the linear mesomeric C≡N acceptor. Surprisingly, attaching strongly withdrawing nitro group (**3e**) increases pK_a to 9.45/21.09. Based on the DFT-optimized structure of **3e** and **1e** (Fig. S3), the reduced acidity is likely ascribed to a strong intramolecular hydrogen bonding between the imidazole N1 and the oxygen atom of the nitro group. In general, the transmission effect of the additional 1,4-phenylene moiety strongly reduces differences in the acidity and decreases pK_a by three/four orders of magnitude (*e.g.* 6.78/15.19 and 3.71/10.96 for **4a** and **3a**). Hence, the acceptor-substituted 1*H*-imidazoles became less acidic (*e.g.* **4a** and **4c**), but the acidity of the donor-substituted ones is pronounced (*e.g.* **4b**). The pronounced acidity is also encountered for 4-nitrophenyl derivative **4e**, confirming the aforementioned assumption on hydrogen bonding of the NO_2 group in **3e**, which is not possible in the extended **4e**. The substituent effects in the series **4a–h** were quantitatively evaluated using the Hammett equation.[52] Well-fitting linear regressions of pK_a *vs.* σ_p (the reaction constant $\rho = -1.55/-2.552$, the correlation coefficient r = 0.968/0.955 and the number of points N = 31/30) were obtained in both solvents (MeOH/ACN). The substituent effects in 2-phenylimidazolides **2a–h** were also investigated using ^{13}C chemical shifts of the imidazolide C2 carbon atom (Table S1). The resulting good linear regressions of δ (^{13}C–C2) *vs.* σ_p (r = 0.981, N = 7, **2b** excluded as an outlier) as well as pK_a of **4a–h** *vs.* δ (^{13}C–C2) of **2a–h** (r = 0.911/0.859, N = 34/35 in MeOH/ACN) confirm an analogous transfer of the electronic effects of the appended substituents R to the imidazol(id)e-4,5-dicarbonitrile moieties, while the electron donating/withdrawing behaviour of the R substituents resembles those of 4-substituted benzoic acid derivatives.

The electronic absorption spectra of lithium salts **1** and **2** (Fig. 2; see also Table 2 for the longest wavelength absorption

Table 1 Average dissociation constants ($\overline{pK}$) and their standard deviations (s) of 1*H*-imidazoles **3** and **4**

	$\overline{pK}(\pm s)^a$	
1*H*-Imidazole	MeOH	ACN
3a	3.71 (0.09)	10.96 (0.11)
3b	8.63 (0.05)	17.92 (0.08)
3c	3.46 (0.03)	9.70 (0.02)
3d	4.94 (0.08)	12.68 (0.13)
3e	9.45 (0.09)	21.09 (0.17)
3f	7.73 (0.04)	16.60 (0.06)
4a	6.78 (0.06)	15.19 (0.12)
4b	7.87 (0.04)	16.98 (0.10)
4c	6.43 (0.07)	14.65 (0.11)
4d	7.48 (0.02)	16.56 (0.04)
4e	6.44 (0.07)	14.69 (0.09)
4f	7.56 (0.02)	16.73 (0.08)
4g	7.52 (0.03)	16.52 (0.09)
4h	8.01 (0.06)	17.18 (0.09)

[a] Determined experimentally *via* potentiometric titration using $Bu_4N^+HO^-$ base and benzoic acid as the standard (pK_0 = 9.41 (MeOH)[50] and 20.70 (ACN)[51]). Average values calculated from 3–5 experiments.

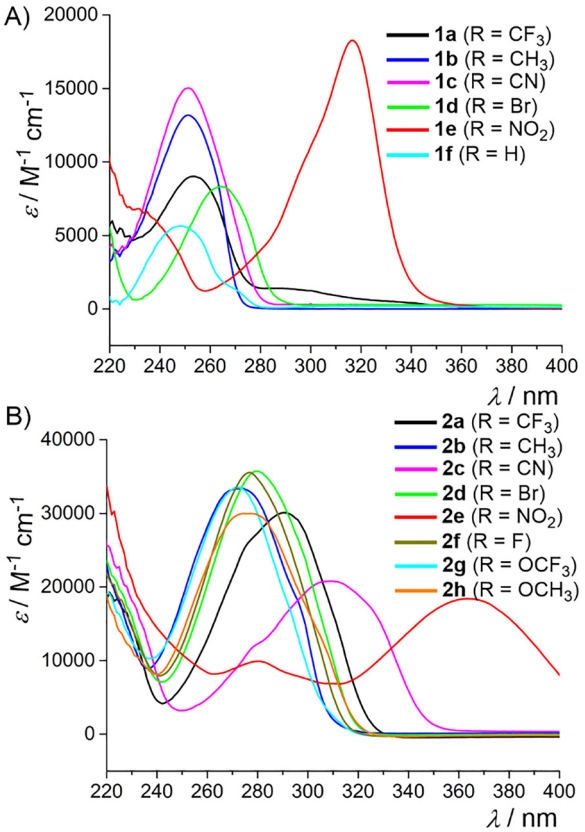

Fig. 2 Electronic absorption spectra of imidazolides: **1** (A) and **2** (B) in DME/DMC (1 : 1) (c = 5 and 2 × 10^{-5} M).

maxima λ^{A}_{max} and the molar absorption coefficients ε) further support the potentiometric measurements. The longest absorption bands in **1a–c** and **1f** are positioned nearly identically and differ mostly in the molar absorption coefficient as a result of attaching either electron acceptor or donor groups (CF_3, CH_3, CN or H). On the contrary, the nitroderivative **1e** showed exceptionally red-shifted absorption maxima, which points to its different structural arrangement. The substituent effects are even more pronounced in the series **2**, where the insertion of the 1,4-phenylene moiety generally red-shifts the absorption maxima by 20–60 nm. The position of the longest wavelength absorption band depends further on the substitution, and the electron acceptors such as CF_3 (**2a**), CN (**2c**) and NO_2 (**2e**) induce the most bathochromically shifted ones. In summary, employing the 1,4-phenylene moiety along with the varied (C2/*para*-)substitution (**a–h**) seems to be a useful strategy to fine-tune the acidity of 1*H*-imidazoles **3** and **4**. The most stabilized conjugated bases (imidazolides **1**/**2**) can be generated from 1*H*-imidazoles **3c**/**3a** and **4a**/**4c**/**4f** bearing CF_3/CN/NO_2 acceptors.

Preparation of electrolytes

Carbonates, (poly)ethers (glymes), esters, amides, sulfones and ionic liquids belong to the most widely employed organic solvents in LIBs.[3,53–55] As an essential prerequisite to their successful application, the solubilities of lithium salts **1** and **2** in dimethyl carbonate (DMC), 1,2-dimethoxyethane (DME) and commercial SolMIX were first screened (Table 2). In all solvents at 25 °C, the benchmark **LiTDI** and $LiPF_6$ showed the largest solubility and up to 1.5/4.8/3.3 and 7.9/1.3/4.9 M solutions can be prepared. The data gathered in DMC further indicate that the salts **1b–f** and **2a–h** are much less soluble or even insoluble with the exception for **2a** and **2g** bearing CF_3 and OCF_3 substituents (solubility up to *ca.* 0.3 M). In contrast to DMC, the solubility in pure DME is significantly enhanced and

Table 2 Summary of the properties of studied imidazolides (**1** and **2**)

Der.	Solubility[a] [g l^{-1}]/[mol l^{-1}] DMC	DME	SolMIX	λ^{A}_{max} [b] [nm eV^{-1}]	ε [b] [M^{-1} cm^{-1}]	T_d [c] [°C]	η [d] [mPa s]	ρ [e] [g cm^{-3}]	E_η [f] [kJ mol^{-1}]	r_s [g] [nm]	r_{eff} [h] [nm]	D [i] [× 10^{-10} m^2 s^{-1}]	κ [j] [mS cm^{-1}]
1a	300/1.56	924/4.81	640/3.30	253/4.90	9000	240	0.884	1.017	14.10	0.548	0.576	4.222	6.33
1b	8/0.06	Insoluble	—	251/4.91	13 200	—	—	—	—	—	—	—	—
1c	Insoluble	300/2.01	—	251/4.91	15 000	—	—	—	—	—	—	—	—
1d	10/0.05	260/1.30	—	264/4.70	8300	—	—	—	—	—	—	—	—
1e	6/0.04	230/1.36	—	317/3.91	18 300	—	—	—	—	—	—	—	—
1f	6/0.05	Insoluble	—	248/5.00	5700	—	—	—	—	—	—	—	—
2a	100/0.37	380/1.42	330/1.23	291/4.26	30 100	260	1.037	1.021	14.21	0.557	0.646	3.205	6.20
2b	Insoluble	600/2.80	20/0.09	273/4.54	33 400	—	1.096	1.008	14.47	0.528	0.670	2.925	3.77
2c	Insoluble	100/0.44	Insoluble	310/4.00	20 800	—	—	—	—	—	—	—	—
2d	Insoluble	720/2.58	80/0.29	280/4.43	35 700	—	—	—	—	—	—	—	—
2e	5/0.02	340/1.39	190/0.78	363/3.42	18 400	—	—	—	—	—	—	—	—
2f	Insoluble	440/2.02	40/0.18	272/4.56	33 500	—	1.060	1.021	14.07	0.568	0.655	3.092	5.93
2g	90/0.32	800/2.82	420/1.48	277/4.48	35 500	190	1.047	1.025	14.34	0.533	0.650	3.154	6.23
2h	Insoluble	440/1.91	Insoluble	277/4.48	30 000	—	1.024	1.007	14.85	0.617	0.641	3.274	3.04
$LiPF_6$	1200/7.90	200/1.32	740/4.87	—	—	180	1.211	1.024	—	—	0.711	2.494	7.87

[a] Determined in dimethyl carbonate (DMC), 1,2-dimethoxyethane (DME) and SolMIX (a commercial mixture of carbonates DMC : EC : EMC, (1 : 1, v/v) at 25 °C using a temperature-tempered ultrasonic bath. [b] Longest wavelength absorption maxima (λ^{A}_{max})/the molar absorption coefficient (ε) measured in DME/DMC (1 : 1) at concentrations of 5 × 10^{-5} (**1**) and 2 × 10^{-5} (**2**). [c] Temperature of endothermic/exothermic decomposition under an inert atmosphere determined by DSC (see Table S2 and Fig. S4). [d] Experimentally measured dynamic viscosity (0.6 M in DME/DMC (1 : 1)) at 20 °C. [e] Experimentally measured densities (0.6 M in DME/DMC (1 : 1)) at 20 °C. [f] Activation energy of viscous flow determined using the Arrhenius equation. [g] Effective solute radius at 20 °C. [h] Effective hydrodynamic radius at 20 °C (c = 0.6 M). [i] Self-diffusion coefficient at 20 °C and c = 0.6 M. [j] Experimentally measured specific conductance (0.6 M in DME/DMC (1 : 1)) at 20 °C. Electrochemical stability windows of the investigated electrolytes were evaluated using linear sweep voltammetry (LSV) from 0 to 5 V (see Fig. 6).

ranges from 0.4 to 2.8 M, including some derivatives practically insoluble in DMC. When comparing salts **1** and **2**, the additional 1,4-phenylene linker in **2** provides enhanced solubility, which further varies based on the substitution. Finally, a 1 : 1 volumetric mixture of DME and DMC and 0.1, 0.3, 0.6 and 1 M concentrations were chosen for further investigation. The electrolytes were freshly prepared in a nitrogen-filled glovebox by dissolving the particular lithium salt in DME and subsequently diluting the solution with DMC. The obtained solubility profiles also served as a primary filter in identifying derivatives with a potential for practical application (**1a**, **2a**/**b** and **2f–h**), while compounds exhibiting poor solubility were excluded from the subsequent investigations. The moisture content is crucial for the overall performance of the prepared electrolytes, and therefore, we determined the water content *via* coulometric titration (using a Karl Fischer titrator) to be below 30 ppm. Compared to benchmark $LiPF_6$, imidazolides **1a**, **2a** and **2g** showed enhanced thermal robustness as measured by DSC (Table 2 and the SI).

Associations and aggregations of electrolytes

Having addressed the formulation of electrolytes, we focused on the behaviour of the selected lithium salts in the DME/DMC solution. We addressed the molecular association and the formation of lower-order aggregates, such as dimers and trimers, as a function of concentration (Fig. 3 and Fig. S5–S12 in the SI). The concentration of **LiTDI** (**1a**) was gradually increased from 10^{-5} M, and the corresponding electronic absorption spectra were recorded (Fig. 3A). We focused especially on tailing of the low-energy region, which is indicative of the Mie scattering effect on the formed aggregates.[56–58] The tailing is evident already at 5×10^{-4} M, which is a significantly lower concentration than that reported for the Raman/FTIR analysis (0.1–0.63 M).[33] At 5×10^{-2} M, a structured new band appearing at around 310–330 nm is clearly visible pointing to the formation of various aggregate types. In contrast to this observation, extended salt **2a** (Fig. 3B) showed only gradually increasing absorbance without any concomitant tailing. Thus, up to 5×10^{-2} M concentration, no formation of aggregates was observed. While **2b**, **2d** and **2h** (Fig. S7, S8 and S11) behave similarly, 4-fluoro (**2f**, Fig. 3C) and 4-trifluormethoxy (**2g**, Fig. S10) derivatives began to form aggregates at around 10^{-3} and 10^{-2} M; the one/two order of magnitude higher concentration than that of benchmark **LiTDI**.

Viscosity and density of electrolytes

Dynamic viscosity and density were measured over the temperature range of −10 to 60 °C with the constant solvent system (DME/DMC = 1 : 1). Table 2 lists the recorded values measured for 0.6 M solutions of **1a**, **2a–b** and **2f–2h** at 20 °C, while Fig. 4 shows exponentially decreasing viscosity and density with the increase in temperature. A rather linear trend is observed especially for the density of the electrolytes of lower concentration (Fig. S12). To assess the temperature dependence of the dynamic viscosity, the activation energy of viscous flow (E_η) was calculated (Table 2 and S3) by linearly fitting η to $1/T$ with the aid of the Arrhenius equation (see the SI and Fig. S13).[59] The increasing E_η values of all derivatives with the increased concentration reflect pronounced intermolecular interactions hindering an efficient viscous flow and further corroborate the aforementioned formation of the clusters and aggregates. However, the viscous flow of the benchmark **LiTDI** substantially depends on the concentration (ΔE_η = 2.77 kJ mol^{-1}; Table S3), which contrasts the relatively steady E_η values measured for **2a** (ΔE_η = 0.97 kJ mol^{-1}). As compared to **LiTDI**, the most efficient viscous flow was recorded for extended derivatives **2a**, **2b**, **2g** and **2h** (0.3 M) possessing a diminished tendency to aggregate as determined by the UV/Vis spectroscopy (see above). Using the Eyring model,[60] the measured dynamic viscosity has further been recalculated to activation parameters of viscous flow such as Gibbs energy of activation ($\Delta G^{\ddagger}$), enthalpy of activation ($\Delta H^{\ddagger}$) and entropy of activation ($\Delta S^{\ddagger}$), see Tables S4, S5 and Fig. S14. The gathered data point to an increased viscous flow with the increase in temperature, while the increasing concentration has expectedly the opposite effect. As compared to other derivatives, salt **2a** showed significantly reduced $\Delta H^{\ddagger}$ and $\Delta S^{\ddagger}$ values at 0.3 M, which may indicate weaker intermolecular interactions and a diminished degree of order, while the positive entropy also points to disorganization during the viscous flow (a disruption of the molecular interactions).

The ionic interactions and solvation effects of the investigated electrolytes were also examined using the Jones–Dole–Kaminsky (JDK) equation[59,61,62] that allows determining the solute effective radius r_s (Table 2 and S6, Fig. S15). While the calculations at 20 °C revealed rather similar r_s values for all derivatives (Table 2), increasing the temperature reduces the radii due to a weakened ion–solvent interaction (a thermal

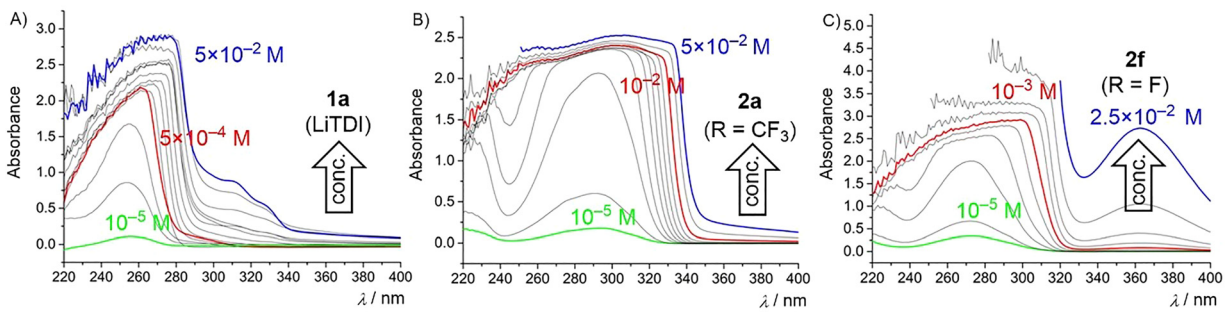

Fig. 3 Representative electronic absorption spectra of lithium salts **1a** (A), **2a** (B) and **2f** (C) with gradually increased concentrations (DME : DMC = 1 : 1).

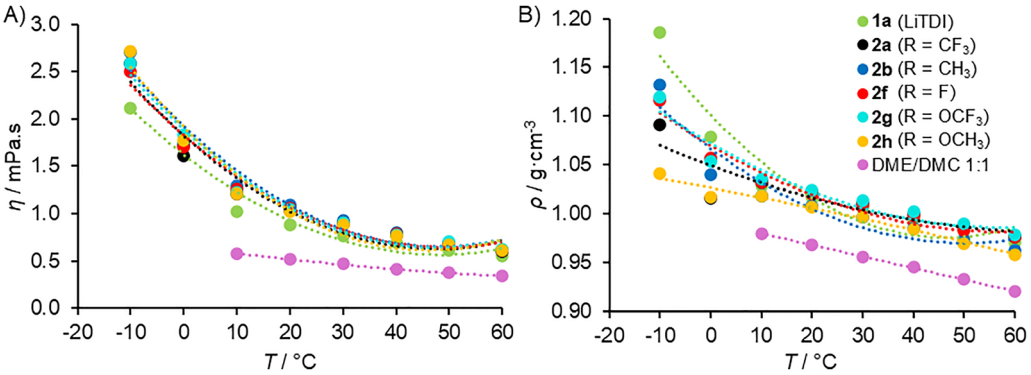

Fig. 4 Dynamic viscosity η (A) and density ρ (B) of imidazolides **1a**, **2a–b** and **2f–h** as a function of temperature (0.6 M solutions in DME/DMC = 1 : 1).

disruption of the solvation shell), see Table S7. A similar trend is seen for the *B* parameter, which also relates to the molar volume. When comparing the benchmark **LiTDI** and **2a**, nearly identical *B* parameters were calculated within the temperature range of 10–60 °C. The electrolyte **2a** shows a relatively steady *D* parameter, compared to its gradually increasing value for **LiTDI**, which points to a nearly temperature-independent ion–ion interaction and highlights the effect of the 1,4-phenylene moiety. Considering the whole series of electrolytes, **2b** (R = CH_3) showed the lowest *B* and the highest *D* parameters, suggesting limited solvation and enhanced ion pairing, while the situation is completely opposite for **2h** (R = OCH_3). This obvious difference demonstrates the influence of the coordinating ether moiety (–O–) in affecting the ion–solvent and ion–ion interactions. Employing complementary Einstein's theory of dilute suspensions,[63,64] the effective hydrodynamic radius r_{eff} was also evaluated (Table 2 and Fig. S16). In contrast to the JDK model focused on localized ion–solvent and ion–ion interactions, the Einstein model includes the solvation shell and aggregates, which is reflected in generally larger r_{eff} values than the r_s values. However, both quantities follow the same trend within the series **2**. The effective hydrodynamic radius has been used to calculate the self-diffusion coefficient *D* (Table 2 and Table S8), characterizing the intrinsic mobility of solvated ions under thermal agitation. Unlike the pulsed-field gradient NMR measurements,[33,59] providing separate diffusion coefficients for cations and anions, this indirect Stokes–Einstein method[65] yields a global average that assumes spherical symmetry and ideal behaviour but is generally considered useful for a comparative study. A comparison of the NMR-estimated $D = 4.25 \times 10^{-10}$ m^2 s^{-1} of **LiTDI** (EC : EMC 3 : 7, 0.6 M, 40 °C)[33] and our $D = 4.22 \times 10^{-10}$ m^2 s^{-1} of **LiTDI** (DME : DMC = 1 : 1, 0.6 M, 20 °C) implies a very good agreement of both methods. In general, the obtained self-diffusion coefficients (Table S8) are highest for **1a**, which reflects its small size compared to derivatives **2** extended by the 1,4-phenylene moiety. However, in diluted 0.1 M solutions, the *D* values for **1a** and **2a** are very close (9.763 *vs.* 9.288 $\times 10^{-10}$ m^2 s^{-1}). The mobility of ions linearly increases with the increase in temperature (Fig. S17), while the increase in viscosity/concentration has the opposite effect (Fig. S18).

Electrochemistry

As expected, the conductometric behaviour of **LiTDI** shows a systematic increase in the ionic conductivity as a function of the increase in concentration (0.1 to 1.0 M, Table S9 and Fig. S19). However, the curvature above c = 0.6 M suggests a diminishing rate caused probably by the growing viscosity and the aggregation phenomena (see above), both reducing the ion mobility. The specific conductance of **1a**, **2a–b** and **2f–2h** measured uniformly for 0.6 M solutions (Table 2) reveals **2a** and **2g** (κ = 6.20 and 6.23 mS cm^{-1}) with nearly identical values as measured for the benchmark **LiTDI** (κ = 6.33 mS cm^{-1}). Thus, the extension of the π-system has not negatively influenced the conductivity. On the contrary, removing the fluorine atom(s) from the R-substituent has detrimental effects, especially for **2b** and **2h** (κ = 3.77 and 3.04 mS cm^{-1}).

To assess the ionic dissociation behaviour of lithium imidazolide salts, the Walden plot was further constructed (Fig. 5 and Table S10). In general, all tested electrolytes deviate below the ideal KCl line, indicating an incomplete dissociation and the presence of ion pairing or aggregation. The data for **LiTDI** at low concentrations (0.1–0.3 M) substantially deviate from the ideal Walden function, whereas the 0.6 and 1 M solutions lie closer. This trend is accompanied by an atypical increase in the ionicity with the increase in concentration (from 2.6 to 9.3%) and a corresponding reduction in the vertical offset ΔW from −1.580 to −1.030. This observation contrasts the behaviour generally reported for carbonate-based electrolytes[26,33] and suggests that, in an ether–carbonate medium, a gradual salt addition enhances ionic mobility or partial dissociation. According to the study of Forsyth *et al.*,[66] using a binary ether-rich mixture leads to a breakdown of the extended ion networks and a faster ion-exchange, most probably due to the σ-donor character of the oxygen atoms of DME.[67] In addition, we would further highlight the lower viscosity/density of DME (η/ρ = 0.4341/0.8665 mPa s^{-1}/g cm^{-3}) as compared to DMC (η/ρ = 0.585/1.0635 mPa s^{-1}/g cm^{-3}), while their 1 : 1 mixture possesses η/ρ = 0.5133/0.9679 mPa s^{-1}/g cm^{-3} at 20 °C. Anyway, a complete dissociation has not been achieved independently on the concentration, which is in line with the current literature data on similar Hückel-type lithium salts.[16,68] When focusing on the structural variation in **2a–b** and **2f–h** at the steady

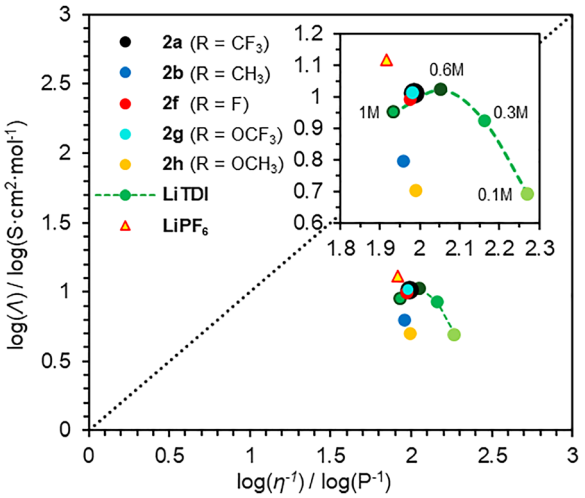

Fig. 5 Molar conductivity (Λ) *versus* inverse dynamic viscosity (η^{-1}) for lithium imidazolide-based electrolytes (**2a,b** and **2f–2h** at 0.6 M; **1a** at 0.1, 0.3, 0.6 and 1.0 M) compared to $LiPF_6$ in DME/DMC (1 : 1) at 20 °C. The dotted line represents the ideal Walden line (fully dissociated KCl). An extended area is also provided as an inset.

concentration (0.6 M), **2a** and **2g** showed the smallest deviations from the ideality (−0.970 and −0.964) corresponding to the highest ionicity (over 10.7%). On the contrary, nonfluorinated salts **2b** and **2h** exhibited pronounced deviations (−1.162 and −1.285) and lower ionicity (6.9 and 5.2%). This suggest a higher concentration of free extended anions **2a**, **2f** and **2g** as compared to the benchmark **1a** as well as the nonfluorinated imidazolides **2b** and **2h**.

Alongside the conductometry, the EIS was performed within the range of 50–200 000 Hz using a conductivity probe. The electrochemical impedance analysis revealed a pronounced dependence of the Randles circuit parameters of **LiTDI** within the concentration range of 0.1–1.0 M (Table 3). Increasing the concentration systematically reduces the solution resistance (R_1) from 1553 to 106.8 Ω, reflecting an enhanced ionic conductivity. The charge-transfer resistance (R_2) decreases by more than five orders of magnitude (422 → 0.005 Ω), indicating a substantial improvement in the interfacial reaction kinetics at a higher ionic strength. The double-layer capacitance (C_1) increases from a few nF to several tens of μF, which is consistent with a compression of the electrical double layer and shortening of the Debye length. The Warburg coefficient (W_1) is highest at 0.1 M and stabilizes thereafter, suggesting that the diffusion limitations are significant only at low concentrations of **LiTDI**. These observations confirm that the transport and interfacial processes dominate under dilute conditions, whereas the system approaches an ideal behaviour with minimal polarization losses at higher concentrations. The EIS measurements of **2a** and **2g** (0.6 M) point to a slightly lower bulk conductivity (R_1 ~ 240 Ω) compared to **LiTDI** (R_1 = 150.9 Ω at the same concentration), but their charge-transfer resistances remain very low (0.016/0.013 Ω for **2a**/**2g**) and comparable to **LiTDI**, suggesting that the interfacial kinetics is not significantly compromised upon extending the π-system

Table 3 Parameter estimated for Randles equivalent circuit model from the EIS data measured for **1a**, **2a** and **2g** in DME : DMC (1 : 1)

Salt (concentration [mol l^{-1}])	R_1 [Ohm]	R_2 [Ohm]	W_1 [Ω $s^{-\frac{1}{2}}$]	C_1 [F]
1a (0.1)	1553	422.3	2330	3.888×10^{-9}
1a (0.3)	378.0	0.023	1492	2.459×10^{-5}
1a (0.6)	150.9	0.007	1575	3.391×10^{-5}
1a (1.0)	106.8	0.005	1575	3.737×10^{-5}
2a (0.6)	242.3	0.016	1561	3.386×10^{-5}
2g (0.6)	240.2	0.013	1253	2.952×10^{-5}

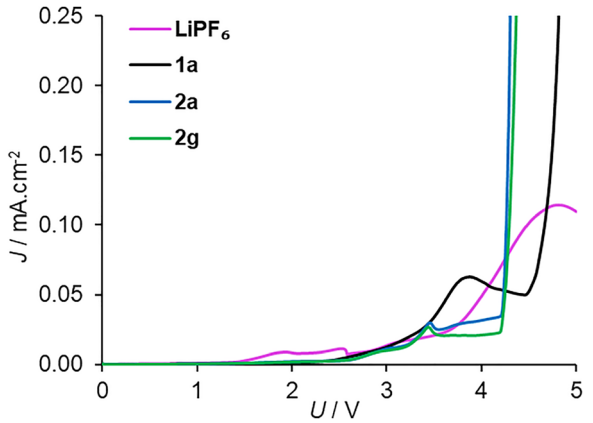

Fig. 6 LSV curves for **LiTDI**, **2a** and **2g** along with the benchmark $LiPF_6$ [0.6 M solutions in DME : DMC (1 : 1)].

or embedding the oxygen atom (CF_3 → OCF_3). The nearly identical double-layer capacitance of both salts and **LiTDI** (~30–34 μF) confirms similar surface characteristics and effective electrode wetting. The lowest Warburg coefficient deduced for **2g** (1253 Ω $s^{-1/2}$), as compared to **2a** and **LiTDI** (1561 and 1575 Ω $s^{-1/2}$), may indicate slightly improved ion diffusion for **2g**.

Linear sweep voltammetry (LSV) was employed to evaluate the electrochemical stability window of imidazolides **2a**, **2g** and **LiTDI** and compare them with the benchmark $LiPF_6$ in a DME : DMC solvent mixture (Fig. 6). All salts exhibited very low background current densities up to approximately 4 V, indicating negligible parasitic reactions and good electrochemical stability within this potential range. When increasing the potential above 4 V, both **2a** and **2g** show a sharp current increase at around 4.2 V, suggesting a slightly lower oxidative limit compared to **LiTDI** (~4.6 V). $LiPF_6$ displays a similar trend to **LiTDI** but with a slightly earlier and more moderate increase in the current density.

Conclusion

In this work, we synthesized fourteen lithium (2-phenyl)-4,5-dicyanoimidazolides with varied peripheral pendants (CF_3, CH_3, CN, Br, NO_2, H, F, OCH_3 and OCF_3). Starting from the diaminomaleonitrile, the used synthetic method relies on straightforward cyclocondensation/oxidation followed by a reaction with lithium hydride. The substituent effects in the prepared 1*H*-imidazoles were examined by potentiometrically determined dissociation constants proving large tunability of their acidity.

The pK_a values measured in methanol range from 3 to 10, while even large differences were found in acetonitrile. The substituent effects of the imidazolides **1** and **2** investigated by ^{13}C NMR and electronic absorption spectra further confirmed the stability of the corresponding conjugated bases as a function of their substitution. The CF_3, CN and NO_2 groups proved to be the most beneficial in this respect. Traditional dimethyl carbonate along with 1,2-dimethoxyethane solvents was utilized to prepare electrolytes, and the latter solvent showed significantly enhanced solubilization of the prepared salts **1** and **2**. The particular derivatives **1a**, **2a**/**b** and **2f–h** were identified as sufficiently soluble in a DMC : DME 1 : 1 mixture, and their solutions were further examined for the association and aggregation phenomena. By employing the electronic absorption spectra, substantially more sensitive methodology addressing aggregation is presented. Especially the extended 2-(4-trifluoromethylphenyl)-4,5-dicyanoimidazolide **2a** showed no aggregation up to 5×10^{-2} M concentration, which is in line with its nearly concentration/temperature-independent viscous flow and ion–ion interactions. Despite their comparable molecular volume, effective hydrodynamic radius and self-diffusion coefficient, the benchmark **LiTDI** aggregates already at 5×10^{-4} M and possesses a concentration/temperature-dependent viscous flow. Compared to **LiTDI** (κ = 6.33 mS cm^{-1}), the extended derivatives **2a** and **2g** bearing CF_3 and OCF_3 peripheral substituents possess nearly the same specific conductance of 6.20 and 6.23 mS cm^{-1}. A significant drop in the κ values is seen upon removing the fluorine atom(s). The Walden plot revealed the highest ionicity ($\sim$10.7%) for **2a** and **2g**, larger than that for **LiTDI** (9.3%), while the EIS and LSV measurements suggest slightly higher ohmic resistance ($\sim$240 *vs.* 151 Ω) and slightly lower oxidative limit (4.2 *vs.* 4.6 V) as compared to **LiTDI**. However, the charge-transfer resistance and the double-layer capacitance are nearly identical, while the lowest Warburg coefficient of **2g** implies again higher ion diffusion. In summary, the systematically evaluated structure of lithium imidazolides **1** and **2** allowed identifying the π-system extension (1,4-phenylene moiety) and variation of the peripheral substituents (R) as a suitable tool to design stabilized anions and electrolytes of LIBs. While the π-system extension and substitution by electron-withdrawing R-substituents help to delocalize the imidazolide electron excess, the fluorine-bearing substituents generally improve the solubility of the ionic salts in an aprotic media of low polarity. The new imidazolides **2a** and **2g** maintain good interfacial performance and diffusion behaviour and their wide electrochemical window makes them suitable for LIBs based on LFP/LMFP or NMC and graphite with a maximal potential of 4.2 V. Moreover, the synthesis of **2a**/**g** starts from the inexpensive and readily available 4-substituted benzaldehydes **8a**/**g**, affording the imine intermediates **7a**/**g** smoothly, while the subsequent oxidation to **4a**/**g** utilizes inexpensive molecular iodine. This contrasts to the synthesis of **LiTDI** using a large excess of toxic TFAA, elevated temperatures and subsequent laborious isolation.

Author contributions

Daniel Pokorný: investigation, methodology, formal analysis, writing – original draft. Tomáš Syrový: investigation, methodology, funding acquisition, writing – original draft. Milan Klikar: investigation. Patrik Pařík: investigation. Zuzana Burešová: investigation. Lenka Řeháčková: investigation. Filip Bureš: writing – review & editing, supervision, project administration, funding acquisition, conceptualization.

Conflicts of interest

There are no conflicts to declare.

Data availability

The data supporting this article have been included as part of the supplementary information (SI). Supplementary information: synthesis, dissociation constant and substitution effects, thermal characterization, aggregation, viscosity and density, electrochemical measurements, and NMR and HR-MS spectra. See DOI: https://doi.org/10.1039/d6ma00187d.

Acknowledgements

This work was supported by the Technology Agency of the Czech Republic (TK04030083, EllyteMat). L. Ř. is indebted to the European Union under the REFRESH – Research Excellence for Region Sustainability and High-tech Industries project (CZ.10.03.01/00/22_003/0000048) *via* the Operational Programme Just Transition.

References

1 F. Wu, J. Maier and Y. Yu, *Chem. Soc. Rev.*, 2020, **49**, 1569.
2 E. R. Logan and J. R. Dahn, *Trends Chem.*, 2020, **2**, 354.
3 Y.-K. Liu, C.-Z. Zhao, J. Du, X.-Q. Zhang, A.-B. Chen and Q. Zhang, *Small*, 2023, **19**, 2205315.
4 A. Hammami, N. Raymond and M. Armand, *Nature*, 2003, **424**, 635.
5 W. Jianwu, Y. Yan and C. Chunhua, *Mater. Express*, 2012, **2**, 197.
6 D. Lisbona and T. Snee, *Process Saf. Environ. Prot.*, 2011, **89**, 434.
7 S. C. Levy, *J. Power Sources*, 1997, **68**, 75.
8 C. L. Campion, W. Li and B. L. Lucht, *J. Electrochem. Soc.*, 2005, **152**, A2327.
9 R. Wagner, N. Preschitschek, S. Passerini, J. Leker and M. Winter, *J. Appl. Electrochem.*, 2013, **43**, 481.
10 N. von Aspern, G.-V. Röschenthaler, M. Winter and I. Cekic-Laskovic, *Angew. Chem., Int. Ed.*, 2019, **58**, 15978.
11 P. G. Balakrishnan, R. Ramesh and T. P. Kumar, *J. Power Sources*, 2006, **155**, 401.
12 J. Arai, A. Matsuo, T. Fujisaki and K. Ozawa, *J. Power Sources*, 2009, **193**, 851.
13 M. Amereller, T. Schedlbauer, D. Moosbauer, C. Schreiner, C. Stock, F. Wudy, S. Zugmann, H. Hammer, A. Maurer, R. M. Gschwind, H.-D. Wiemhöfer, M. Winter and H. J. Gores, *Prog. Solid State Chem.*, 2014, **42**, 39.

14 Y. Cai, H. Zhang, Y. Cao, Q. Wang, B. Cao, Z. Zhou, F. Lv, W. Song, D. Duo and L. Yu, *J. Power Sources*, 2022, **535**, 231481.
15 Z. Li, L. Wang, X. Huang and X. He, *Adv. Funct. Mater.*, 2024, **34**, 2408319.
16 M. Armand, P. Johansson, M. Bukowska, P. Szczeciński, L. Niedzicki, M. Marcinek, M. Dranka, J. Zachara, G. Żukowska and M. Marczewski, *J. Electrochem. Soc.*, 2020, **167**, 070562.
17 M. E. Easton, H. Choudhary and R. D. Rogers, *Chem. – Eur. J.*, 2019, **25**, 2127.
18 M. Egashira, B. Scrosati, M. Armand, S. Béranger and C. Michot, *Electrochem. Solid-State Lett.*, 2003, **6**, A71.
19 P. Johansson, S. Béranger, M. Armand, H. Nilsson and P. Jacobsson, *Solid State Ionics*, 2003, **156**, 129.
20 D. W. McOwen, S. A. Delp, E. Pillard, C. Herriot, S.-D. Han, P. D. Boyle, R. D. Sommer and W. A. Henderson, *J. Phys. Chem. C*, 2014, **118**, 7781.
21 M. Bukowska, J. Prejzner and P. Szczeciński, *Pol. J. Chem.*, 2004, **78**, 417.
22 L. Niedzicki, G. Z. Żukowska, M. Bukowska, P. Szczeciński, S. Grugeon, S. Laruelle, M. Armand, S. Panero, B. Scrosati, M. Marcinek and W. Wieczorek, *Electrochim. Acta*, 2010, **55**, 1450.
23 L. Niedzicki, M. Kasprzyk, K. Kuziak, G. Z. Żukowska, M. Marcinek, W. Wieczorek and M. Armand, *J. Power Sources*, 2011, **196**, 1386.
24 L. Niedzicki, S. Grugeon, S. Laruelle, P. Judenstein, M. Bukowska, J. Prejzner, P. Szczeciński, W. Wieczorek and M. Armand, *J. Power Sources*, 2011, **196**, 8696.
25 L. Niedzicki, E. Karpierz, A. Bitner, M. Kasprzyk, G. Z. Zukowska, M. Marcinek and W. Wieczorek, *Electrochim. Acta*, 2014, **117**, 224.
26 C. L. Berhaut, P. Porion, L. Timperman, G. Schmidt, D. Lemordant and M. Anouti, *Electrochim. Acta*, 2015, **180**, 778.
27 C. L. Berhaut, R. Dedryvère, L. Timperman, G. Schmidt, D. Lemordant and M. Anouti, *Electrochim. Acta*, 2019, **305**, 534.
28 F. Lindgren, C. Xu, L. Niedzicki, M. Marcinek, T. Gustafsson, F. Björefors, K. Edström and R. Younesi, *ACS Appl. Mater. Interfaces*, 2016, **8**, 15758.
29 C. Xu, S. Renault, M. Ebadi, Z. Wang, E. Björklund, D. Guyomard, D. Brandell, K. Edström and T. Gustafsson, *Chem. Mater.*, 2017, **29**, 2254.
30 F.-M. Wang, S. A. Pradanawati, N.-H. Yeh, S.-C. Chang, Y.-T. Yang, S.-H. Huang, P.-L. Lin, J.-F. Lee, H.-S. Sheu, M.-L. Lu, C.-K. Chang, A. Ramar and C.-H. Su, *Chem. Mater.*, 2017, **29**, 5537.
31 J. Sheers, P. Johansson, P. Szczeciński, W. Wieczorek, M. Armand and P. Jacobsson, *J. Power Sources*, 2010, **195**, 6081.
32 T. Sriana, E. G. Leggesse and J. C. Liang, *Phys. Chem. Chem. Phys.*, 2015, **17**, 16462.
33 A. Szczęsna-Chrzan, M. Vogler, P. Yan, G. Z. Żukowska, C. Wölke, A. Ostrowska, S. Szymańska, M. Marcinek, M. Winter, I. Cekic-Laskovic, W. Wieczorek and H. S. Stein, *J. Mater. Chem. A*, 2023, **11**, 13483.
34 C. C. Su and K. Amine, *US Pat.*, 20240396089A1, 2024.
35 M. Armand, S. Gruegon, S. Laruelle, M. Bukowska, P. Szczecinski, W. Wieczorek, L. Niedzicky, B. Scrosati, S. Panero and P. Realle, *US Pat.*, 9452987B2, 2016.
36 T. L. Dzwiniel and K. Z. Pupek, *US Pat.*, 20230406828A1, 2023.
37 K. Zaghib, M. Beaupre, C. Mallet, J.-C. Daigle, Y. Asakawa and S. Uesaka, *WO Pat.*, 2019006560A1, 2019.
38 C. Mellet, S. Rochon, A. Lafleur-Lambert, S. Uesaka and K. Zaghib, *WO Pat.*, 2018176137A1, 2018.
39 P. G. Rasmussen, R. L. Hough, J. E. Anderson, O. H. Bailey and J. C. Bayon, *J. Am. Chem. Soc.*, 1982, **104**, 6155.
40 H. Wang, C. Zhao, Z. Burešová, F. Bureš and J. Liu, *J. Mater. Chem. A*, 2023, **11**, 3753.
41 J. Kulhánek, F. Bureš, O. Pytela, T. Mikysek, J. Ludvík and A. Růžička, *Dyes Pigm.*, 2010, **85**, 57.
42 J. Kulhánek and F. Bureš, *Beilstein J. Org. Chem.*, 2012, **8**, 25.
43 A. Plaquet, B. Champagne, J. Kulhánek, F. Bureš, E. Bogdan, F. Castet, L. Ducase and V. Rodriguez, *ChemPhysChem*, 2011, **12**, 3245.
44 N. Dey, J. Kulhánek, F. Bureš and S. Bhattacharya, *J. Org. Chem.*, 2019, **84**, 1787.
45 J. Kulhánek, F. Bureš, J. Opršal, W. Kuznik, T. Mikysek and A. Růžička, *Asian J. Org. Chem.*, 2013, **2**, 422.
46 F. Bureš, *RSC Adv.*, 2014, **4**, 58826.
47 M. Ludwig, O. Pytela, K. Kalfus and M. Večeřa, *Collect. Czech. Chem. Commun.*, 1984, **49**, 1182.
48 M. Ludwig, O. Pytela and M. Večeřa, *Collect. Czech. Chem. Commun.*, 1984, **49**, 2593.
49 M. Ludwig, O. Pytela and M. Večeřa, *Collect. Czech. Chem. Commun.*, 1986, **51**, 1948.
50 I. M. Kolthoff and L. S. Guss, *J. Am. Chem. Soc.*, 1938, **60**, 2316.
51 I. M. Kolthoff and M. K. Chantooni, Jr., *J. Am. Chem. Soc.*, 1971, **93**, 3843.
52 O. Exner, *Correlation Analysis of Chemical Data*, Plenum, New York, 1988, pp. 61–62.
53 M. Watanabe, K. Dokko, K. Ueno and M. L. Thomas, *Bull. Chem. Soc. Jpn.*, 2018, **91**, 1660.
54 E. O. Nachaki and D. G. Kuroda, *J. Phys. Chem. B*, 2024, **128**, 3408.
55 S. Tan, Y. J. Ji, Z. R. Zhang and Y. Yang, *ChemPhysChem*, 2014, **15**, 1956.
56 A. J. Cox, A. J. DeWeerd and K. Linden, *Am. J. Phys.*, 2002, **70**, 620.
57 R. S. Fernandes, S. Paul, J. Tydlitát, F. Bureš and N. Dey, *J. Org. Chem.*, 2024, **89**, 17926.
58 S. K. Behera, A. Murkherjee, G. Sadhuragiri, P. Elumalai, M. Sathiyendrian, M. Kumar, B. B. Mandal and G. Krishnamoorthy, *Faraday Discuss.*, 2017, **196**, 71.
59 C. L. Berhaut, D. Lemordant, P. Porion, L. Timperman, G. Schmidt and M. Anouti, *RSC Adv.*, 2019, **9**, 4599.
60 L. J. dos Santos, L. A. Espinoza-Velasquez, J. A. P. Coutinho and S. Monteiro, *Fluid Phase Equilib.*, 2020, **522**, 112774.
61 G. Jones and M. Dole, *J. Am. Chem. Soc.*, 1929, **51**, 2950.

62 J. Jiang and S. I. Sandler, *Ind. Eng. Chem. Res.*, 2003, **42**, 6267.
63 S. Uchida and T. Kiyobayashi, *Phys. Chem. Chem. Phys.*, 2021, **23**, 10875.
64 S. G. Schultz and A. K. Solomon, *J. Gen. Physiol.*, 1961, **44**, 1189.
65 S. Berkowicz and F. Perakis, *Phys. Chem. Chem. Phys.*, 2021, **23**, 25490.
66 U. Pal, F. Chen, D. Gyabang, T. Pathirana, B. Roy, R. Kerr, D. R. MacFarlane, M. Armand, P. C. Howlett and M. Forsyth, *J. Mater. Chem. A*, 2020, **8**, 18826.
67 G. Comas-Vilà and P. Salvador, *ChemPhysChem*, 2024, **25**, e202400582.
68 D. Farhat, D. Lemordant, J. Jacquemin and F. Ghamouss, *J. Electrochem. Soc.*, 2019, **166**, A3487.